

# Calculated Pulse Widths and Spectra of a Single Sonoluminescing Bubble

William C. Moss,\* Douglas B. Clarke, David A. Young

A sonoluminescing bubble has been modeled as a thermally conducting, partially ionized, two-component plasma. The model shows that the measured picosecond pulse widths are due to electron conduction and the rapidly changing opacity of the plasma and that these mechanisms are also responsible for the absence of an "afterglow" subsequent to the sonoluminescence flash while the hot bubble expands and cools. The calculated spectra for sonoluminescing nitrogen and argon bubbles suggest that a sonoluminescing air bubble probably contains only argon, in agreement with a recent theoretical analysis.

Sonoluminescence (SL) arises from the nucleation, growth, and collapse of gas-filled bubbles in a liquid. A single acoustically levitated and trapped bubble (1, 2) exhibits SL characterized by light emission that is synchronous with the periodic acoustic driving field, has a measured pulse width of  $\leq 50$  ps (3), and displays emission spectra consistent with that of a  $\geq 2$ -eV blackbody radiator (4). Although a definitive theoretical explanation of the acoustical-to-optical energy conversion is still lacking, numerical hydrodynamic simulations (5, 6) suggest that shock waves generated during the collapse of the bubble can produce the short measured pulse widths and the inferred high temperatures. Additional support for the shock model comes from the experimental detection and numerical simulation of an acoustic pulse in the liquid near the bubble within 1  $\mu$ s after the flash, which is presumably the rebound of the shock from the center of the bubble (7).

Correct theoretical predictions of the measured pulse widths constitute a minimum requirement for any proposed model. Unfortunately, the measurements give only an upper bound, which is a weak constraint. A more comprehensive numerical validation of a model requires simulations of more accurately known quantities, such as spectra and the dependence of the optical output and pulse width on the type of gas in the bubble (4, 8). Calculation of these phenomena are beyond the capabilities of any previous theoretical models of SL.

If we assume that shock compression heats the bubble so that the emitted light is due to thermal emission from a radiating, partially ionized plasma, then additional physics beyond that described in the single-temperature hydrodynamic conservation equations (5, 6, 9) and accurate high-tem-

perature and high-pressure equations of state (6) is needed. What is required is that the partially ionized plasma be described by distinct but coupled ion and electron temperature fields, with associated losses by plasma thermal conduction, an emission model for coupling the matter energy to the radiation field, and a model for the opacity of the radiating matter.

We show here that a collapsing bubble that is described by the partially ionized plasma model described above provides an explanation of many features of single-bubble SL (SBSL) that have not been collectively accounted for in earlier models. In particular, our calculations show that (i) the optical pulse width and spectra are very sensitive to the maximum bubble radius, which is controlled by the applied acoustic pressure; (ii) the emitted light is described by neither a pure Planckian nor a pure bremsstrahlung spectrum, but a convolution of the two; (iii) the spectral flux of nitrogen ( $N_2$ ) SBSL is approximately 1/25 that of air, which agrees with experimental measurements (8); (iv) the spectrum of argon (Ar) SBSL is nearly identical to the measured spectrum of air SBSL, which suggests that a sonoluminescing air bubble is actually an Ar bubble (10) undergoing SL and may also explain why SBSL in noble gases is more intense than in diatomic gases (8); (v) electron conduction and the opacity are the mechanisms responsible for the picosecond duration of SBSL; and (vi) after the main flash there cannot be an "afterglow" emitted by the expanding hot bubble (11).

We first qualitatively describe the physics in our model to simplify the interpretation of the quantitative results. During the collapse of the bubble, a shock is generated that compresses and heats the contents of the bubble. More heating occurs at the center of the bubble than at its boundary because the shock strength increases as it approaches the bubble's center. The hotter regions begin to ionize and create a two-component plasma of ions and electrons.

The hot matter emits light by an energy cascade from the ions, to the electrons, to the photons. Although work is done on both the ions and the electrons as the bubble collapses, the mechanical energy from the shock goes only into the ions (12); this can create high ion temperatures but relatively low electron temperatures. Because of the high density ( $\rho \sim 1 \text{ g cm}^{-3}$ ), the self-collision times of the ions and electrons are very short (on the order of femtoseconds or less) (12), so that the ions and electrons are each self-equilibrated; that is, the ions and electrons can each be described by a spatially and temporally varying Maxwellian distribution represented by an ion temperature  $T_i(r, t)$  and an electron temperature  $T_e(r, t)$ , where  $r$  is the radial distance from the center of the bubble and  $t$  is time. The ions and electrons exchange energy collisionally, so after a few collisions  $T_i$  equals  $T_e$ . The ion-electron collision time is at least 40 times greater than either of the self-collision times (12), which is still very short, even compared to picosecond SL, so that  $T_i \neq T_e$  occurs only very briefly and does not affect the results discussed here (13). Nevertheless, we still need to treat the ions and electrons separately because losses by plasma thermal conduction occur at very different rates in the ions and electrons. Normal atomic thermal conduction is proportional to  $T^{1/2}$  and is much slower than plasma thermal conduction, which is proportional to  $T_i^{5/2} Z^{-4} M_i^{-1/2}$  for ions and  $T_e^{5/2} Z^{-1} M_e^{-1/2}$  for electrons, where  $Z$ ,  $M_i$ , and  $M_e$  are, respectively, the ion charge, ion mass, and electron mass (12). Electron conduction is typically the dominant energy loss mechanism because of the mass term, and we show below that it has a significant influence on the calculated optical pulse width.

In the final step of the cascade, the electrons lose energy to the photon field to produce the SL flash. The electron-photon coupling can be due to bremsstrahlung, Compton scattering, photo-ionization, and line transitions. However, for what we believe to be typical SBSL conditions, bremsstrahlung is probably the dominant mechanism (14). Our calculations show that light is emitted from regions that are optically thick and thin. If the emitting region is optically thick, then the coupling mechanism is irrelevant. The emitted optical energy flux comes only from the surface of the region and can be calculated from the blackbody expression  $\sigma T_e^4$ , where  $\sigma$  is the Stefan-Boltzmann constant. However, if the region is optically thin, then the coupling mechanism is important and the emitted optical power is a volume integral of the emissivity, which is proportional to the product of a source function and the com-

Lawrence Livermore National Laboratory, Post Office Box 808, Livermore, CA 94550, USA.

\*To whom correspondence should be addressed.  
E-mail: wmoss@llnl.gov

bined opacities (inverse density times the inverse photon mean free path) of the coupling mechanisms (9). Unfortunately, it is difficult to calculate the electron-photon coupling and the source function in a partially ionized plasma, because the plasma is too hot to be described accurately by "cold physics" and too cold to be described accurately by "hot physics." Despite this difficulty, the emission calculation for an optically thin emitter can be simplified greatly if the matter and photon field satisfy certain conditions, which we describe next.

Typical SBSL spectra (4, 8) can be integrated to show that the energy per flash is at most one-millionth of the thermal energy in the compressed bubble. Consequently, the photon field cannot affect the matter field. (The temperature would have to be more than two orders of magnitude higher for the photon and matter fields to have comparable energies.) The combination of the insensitivity of the matter field to the photon field and the properties of the matter being dominated by collisions creates a condition of local thermodynamic equilibrium (LTE). This condition constrains the source function to be the Planck function, whether or not the photon field is in equilibrium with the matter field, so that the emissivity of the matter is proportional to the product of the opacity and the Planck function (9, 15). Consequently, the calculated spectrum from an optically thin plasma in LTE is a convolution of the spectra associated with the electron-photon coupling mechanism (such as bremsstrahlung) and a blackbody. It resembles neither a pure bremsstrahlung nor a pure blackbody spectrum. The simplification introduced by LTE allows the emitted optical power to be computed entirely from the properties of the matter, specifically  $\rho$ ,  $T_e$ , and the opacity  $\kappa$ , which is a function of  $\rho$ ,  $T_e$ , and the photon frequency  $\nu$ . This completes our qualitative description of the energy cascade in a bubble undergoing SL.

We assume spherical symmetry and consider the motion of a bubble filled with  $N_2$  or Ar gas with initial radius  $R_0$  surrounded by a shell of water, whose outer radius is  $R_w$ . The gas and water are initially at atmospheric pressure,  $P_0 = 1$  bar, in thermal equilibrium at room temperature, and at rest. The outer radius of the water is driven by an oscillatory pressure  $P_0 - P_a \sin \omega t$ , where  $P_a$  is the applied acoustic pressure and  $\omega$  is its frequency of oscillation. We calculate the bubble's response to only one cycle of the driving oscillatory pressure, that is, only one of the many growth and collapse cycles that the bubble experiences. We assume that the physics that governs the creation of any one of the steady-state SL flashes can be approximated with the

use of typical values for  $R_0$ ,  $R_w$ ,  $\omega$ , and  $P_a$ , because the bubble collapse is primarily an inertial effect of the liquid compressing the gas. Any set of parameters that produces a typical bubble radius, as a function of time, should be sufficient to supply the inertial forces that generate the flash. The parameters we have chosen are typical (16) but not representative of any particular experiment:  $R_0 = 4.5 \mu\text{m}$ ,  $R_w = 3 \text{ cm}$ , and  $\omega = 2\pi(27.6 \text{ kHz})$ . The values of  $P_a$  will be discussed below.

We neglect viscosity, surface tension, normal heat conduction, and mass diffusion, because they have only second-order effects on the energetics of the primary adiabatic collapse of the bubble. Because of LTE, we are able to ignore the photon field energy and the electron-photon coupling. We believe that the physics we have included in our model is sufficiently complete to accurately describe a hot imploding bubble undergoing SL. The resulting equations for the conservation of mass, momentum, and energy for the system are (9, 17)

$$\begin{aligned} \frac{D\rho}{Dt} &= -\rho \nabla \cdot \mathbf{v} \\ \rho \frac{D\mathbf{v}}{Dt} &= -\nabla(P + Q) \\ \rho \frac{DE_i}{Dt} &= -(P_i + Q) \nabla \cdot \mathbf{v} \\ &\quad + \bar{K}_{ie}(T_e - T_i) + \nabla \cdot (K_i \nabla T_i) \\ \rho \frac{DE_e}{Dt} &= -P_e \nabla \cdot \mathbf{v} + \bar{K}_{ie}(T_i - T_e) \\ &\quad + \nabla \cdot (K_e \nabla T_e) \\ P &= P_e(\rho, T_e) + P_i(\rho, T_i) \\ E &= E_e(\rho, T_e) + E_i(\rho, T_i) \end{aligned} \quad (1)$$

where

$$\frac{D}{Dt} \equiv \frac{\partial}{\partial t} + \mathbf{v} \cdot \nabla \quad (2)$$

and  $\rho$ ,  $\mathbf{v}$ ,  $Q(|\nabla \mathbf{v}|^2, \nabla \mathbf{v})$ ,  $P$ , and  $E$  are, respectively, the density, velocity, artificial viscosity (18, 19), pressure, and specific internal energy;  $\bar{K}_{ie}$ ,  $K_i$ , and  $K_e$  represent, respectively, the ion-electron coupling and the ion and electron thermal conductivities. The pressure and energy are partitioned into ionic and electronic components. Equation 1 comprises a simplified description of the LASNEX "hydrocode," which has been used extensively to study inertial confinement fusion (17).

The  $N_2$  gas was described by an analytic equation of state (6) that includes rotational-vibrational excitation, dissociation, ionization, and repulsive and attractive intermolecular potentials. This equation of state was constructed from a

combination of data and theory and is believed to be valid for the densities and temperatures in these calculations. The equation of state is in general a description of material behavior that has no adjustable parameters after it is constructed. The Ar (20) and water (21) equations of state were obtained from more sophisticated models. Simpler models, such as a van der Waals equation of state with a constant specific heat (5), are not valid at the densities and the temperatures that are reached during the final stages of the bubble's collapse (6). The equations of motion (Eq. 1) and the equations of state combined with the boundary and initial conditions given above can be solved for the radial and temporal variation of all the field quantities.

Figure 1 shows the final 80 ps of the simulated collapse of a  $N_2$  bubble;  $P_a$  was set at 0.23 bar, which produces a 44- $\mu\text{m}$  maximum bubble radius ( $R_{\text{max}}$ ). A pressure of  $P_a = 0.23$  bar applied at  $R_w$  produces the 1.5-bar driving pressure near the bubble (22) that is typical for SBSL experiments. The thick solid line shows the time dependence of the bubble radius  $R(t)$ . The thin solid line shows the shock, which reflects from the center of the bubble at  $t = 15$  ps. The value of  $R(t)$  decreases until the reflected shock reaches the gas-liquid interface, after which the divergent shock continues to propagate into the liquid (7) and  $R(t)$  increases. The arrival of the reflected shock at the gas-liquid interface usually is sufficient but not necessary to reverse the collapse of the bubble. The increasing pressure near the gas-liquid interface of a collapsing bubble would eventually cause the radius to begin to increase even without a shock wave. The long dashed and dotted lines show the power emitted between 180

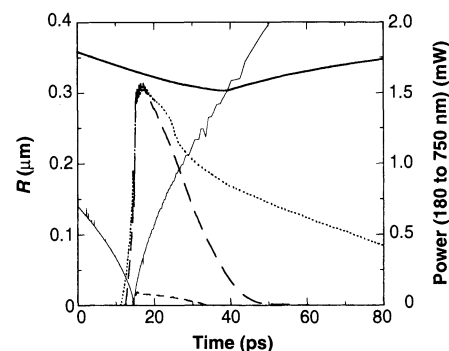


Fig. 1. The final 80 ps of the calculated collapse of a  $N_2$  bubble. The left ordinate shows the time dependence of the bubble radius [ $R(t)$ , thick solid line], shock location [ $R_{\text{sh}}(t)$ , thin solid line], and the shock-induced optically thick region [ $R_{\text{th}}(t)$ , short dashed line]. There is numerical noise in  $R_{\text{sh}}(t)$ . The right ordinate shows the amplitude of the emitted power with (long dashed line) and without (dotted line) losses by plasma thermal conduction.

and 750 nm with and without plasma thermal conduction, respectively. The optical emission begins before the shock reaches the center because of the temperature increase during the collapse and peaks when the shock reflects from the center of the bubble. The reflected shock creates a small optically thick region (short dashed line) near the center of the bubble, but most of the emission is from the optically thin region.

The intensity of the emission and the extent of the optically thick region are controlled by  $\kappa$ , which is a function of the matter density, electron temperature, and photon frequency. There is currently no accurate method to calculate  $\kappa(\nu)$  of a cool ( $<10$  eV), partially ionized dense plasma (23), so an approximate model was constructed for Ar and N<sub>2</sub>. Our calculated electron temperatures never exceed 10 eV, so we obtain an upper bound on the opacity by calculating a density-dependent Rosseland mean opacity that is valid at  $T_e = 10$  eV (24, 25). We assume that the values are constant below 10 eV until the onset of ionization, which in a compressed gas at liquid density begins at approximately 1/4 of the ionization potential (IP) (14) ( $IP_{Ar} = 15.8$  eV,  $IP_{N_2} = 14.5$  eV). We let  $\kappa$  decrease exponentially when the temperature is below  $IP/4$ . The emitted power is calculated with the expression (9)

$$\text{Optical power} = \int \eta(T_e) \sigma T_e^4 dA_{th} + \int_{R_{th}}^R 4\eta(T_e) \rho \kappa(\rho, T_e) \sigma T_e^4 dV \quad (3)$$

where  $T_e$  varies spatially and temporally, and  $\eta$ ,  $A_{th}$ ,  $R$ , and  $R_{th}$  are, respectively, the

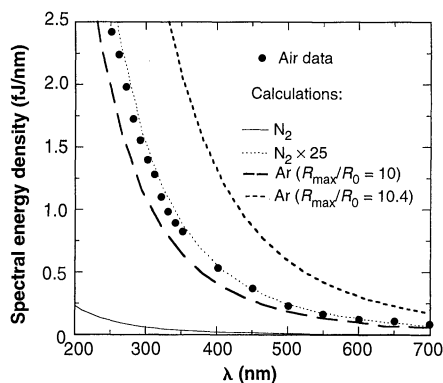


**Fig. 2.** The wavelength ( $\lambda$ ) dependence of the measured SBSL spectrum for air (circles) and calculated spectra for N<sub>2</sub> (solid line) and Ar (long and short dashed lines). The calculated spectrum of an N<sub>2</sub> bubble undergoing SL is only 4% as intense as the measured air spectrum, in agreement with experimental data. The dotted line shows the calculated N<sub>2</sub> spectrum multiplied by 25.

fraction of the Planck spectrum between 180 and 750 nm, the area of the optically thick region, the bubble radius, and the radius of the optically thick region. The quantity  $R_{th}$  is defined by the expression

$$1 = \int_R^{R_{th}} \rho \kappa(\rho, T_e) dr \quad (4)$$

Figure 1 shows that the entire bubble is optically thin ( $R_{th} = 0$ ) except during the time  $15 \text{ ps} < t < 34 \text{ ps}$ .

Electron conduction accounts for the difference between the two optical power curves in Fig. 1. The calculated ion conductive losses are negligible, which agrees with the qualitative description given above. Figure 1 shows that plasma thermal conduction must be included in the analysis; otherwise, the calculated pulse width is longer than the measured upper bound of 50 ps. [Even the emission from a fully ionized plasma produces a calculated pulse width less than 50 ps (not shown)]. The peak output is 1.5 mW:  $3.3 \times 10^4$  photons with a total energy of 0.15 MeV per flash. The light is emitted by only the inner 0.05  $\mu\text{m}$  of the bubble in a 15-ps full-width at half-maximum pulse.

The calculations show that  $T_e(R_{th}, t)$  never exceeds 9 eV. Although the center of the bubble reaches  $T_i = 94$  eV and  $T_e = 29$  eV during the peak optical output, these temperatures cannot be seen outside the bubble;  $T_i = T_e$  everywhere except near the center of the bubble, and both decrease as  $r \rightarrow R$ . When the flash occurs,  $T_e(R) = 0.36$  eV, which is comparable to the temperature due to an isentropic compression of a room-temperature ideal gas (ratio of specific heats  $\gamma = 1.4$ ) from  $R = 4.5$  to  $0.3 \mu\text{m}$ .

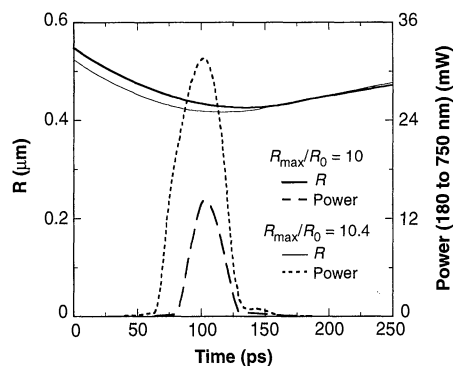


**Fig. 3.** Calculated pulse widths and amplitudes of the emitted power are sensitive to bubble dynamics. Although a difference of only 0.006 bar in driving pressure at the flask (0.07 bar near the bubble) for an Ar bubble produces a small difference in  $R(t)$  ( $R_{max}/R_0 = 10$  versus 10.4), the pulse width and peak amplitude of the emitted power change by more than a factor of 2.

Figure 2 shows the wavelength dependence of the computed spectral content (solid line) for the calculation shown in Fig. 1. The experimental SBSL spectrum for room-temperature air (4) is also shown. Our calculation agrees with the observation that the measured air spectrum is  $\sim 25$  times more intense than the measured N<sub>2</sub> spectrum (8).

Experimental measurements have shown that the intensity of air SBSL is affected strongly by the amount of noble gas (0.9% Ar) in the air (8). The addition of 0.9% Ar has a negligible calculated effect on the optical emission and cannot account for the factor of 25 for the calculated results shown in Fig. 2. Lohse *et al.* (10) have suggested that chemical reactions due to the high temperatures in an air bubble undergoing SL can rectify its contents so that only the chemically inert Ar remains. Figure 3 shows the calculated optical emission (long dashed line) and  $R(t)$  (thick solid line) of a collapsing Ar bubble, for a bubble expansion ratio ( $R_{max}/R_0$ ) of 10.0 ( $P_a = 0.234$  bar). The pulse width is 24 ps, with a peak output of 14 mW;  $6 \times 10^5$  photons with a total energy of 2.6 MeV per flash. The calculated spectrum is plotted (long dashed line) in Fig. 2. The agreement of this Ar calculation with the air data is very good. Our calculations show that the entire Ar bubble is optically thin except during the time  $86 \text{ ps} < t < 111 \text{ ps}$  (not shown in Fig. 3), during which time  $T_e(R_{th}, t)$  never exceeds 5 eV. The quantities  $T_i$  and  $T_e$  never differ by more than 0.2 eV, never exceed 7 eV at the center of the bubble, and decrease as  $r \rightarrow R$ . When the flash occurs,  $T_e(R) = 0.8$  eV. This temperature is below the 3-eV temperature of an isentropic compression of an ideal  $\gamma = 5/3$  gas from  $R = 4.5$  to  $0.43 \mu\text{m}$ , because of losses by electron conduction.

We conclude from the preceding discussion that the shock is stronger in the N<sub>2</sub> than in the Ar bubble. It is more difficult to generate a shock in Ar than in N<sub>2</sub>, because Ar has a higher specific heat ratio, 5/3 versus 7/5. This produces higher sound speeds in Ar, for similar compressions, yet the calculated output of the Ar bubble is over 20 times greater than that for the N<sub>2</sub> bubble. Equation 3 shows that the output is proportional to the opacity, which compounds the paradox because the opacity of N<sub>2</sub> is two to three times greater than that of Ar (20, 25). Although the shock is weaker in Ar than in N<sub>2</sub>, the temperature is a stronger function of compression in Ar because of the larger specific heat ratio. Consequently, the Ar bubble is compressed more isentropically than the N<sub>2</sub> bubble and has a lower peak temperature but a higher average temperature. This is confirmed by the calculations, which show that the light is emitted by the inner 0.18  $\mu\text{m}$  of the Ar

bubble, compared to the inner  $0.03 \mu\text{m}$  of the  $\text{N}_2$  bubble. The radiating volume of Ar is  $\approx 220$  times greater than that of  $\text{N}_2$ , and so, despite the opacity differences, the Ar bubble is brighter. This analysis may explain why SBSL is brighter in noble gases than in diatomic gases (8). We believe that these results provide strong support for the hypothesis of Lohse *et al.* (10) that a sonoluminescing air bubble contains mostly Ar.

The calculated spectra and power are sensitive to small changes in the expansion ratio, which also correspond to moderate changes in the amplitude of the driving pressure near the bubble. The short dashed lines in Figs. 2 and 3 show the calculated results for an Ar bubble with  $R_{\text{max}}/R_0 = 10.4$ . The two expansion ratios represent only a 0.006-bar difference in the driving pressure at the flask, which equals a 0.07-bar difference in the driving pressure near the bubble (22). Although the  $R(t)$  values are similar, the pulse width (24 ps versus 43 ps), the peak amplitude of the emitted power (14 mW versus 32 mW), the number of photons per flash (0.6 million versus 1.9 million), and the spectra are sensitive to  $R_{\text{max}}/R_0$  (the driving pressure). Experimental data exhibit this same sensitivity (26). This result suggests that the reported sensitivities of SBSL to various parameters may be difficult to analyze quantitatively without concomitant measurements of  $R_0$  and  $R_{\text{max}}/R_0$  for each experiment.

The photon emission rate for the  $R_{\text{max}}/R_0 = 10.0$  Ar calculation has a peak value of  $2 \times 10^4 \text{ ps}^{-1}$  at  $t = 103 \text{ ps}$  and a value of  $10 \text{ ps}^{-1}$  at  $t = 200 \text{ ps}$ . It has been speculated that, after the "flash," there still should be visible radiation from the hot bubble as it expands and cools. Our model predicts that this afterglow will not occur, in agreement with experimental data (11). Equation 3 shows that an optically thin plasma cannot radiate if its opacity is low, even if its temperature is high. When the temperature in the bubble drops below  $IP/4$ , the opacity in our model drops precipitously, which terminates the flash and all subsequent optical emission. Consequently, there is no afterglow as the bubble expands and cools. Our calculations show that the short pulse width and lack of afterglow are intimately related and are due to electron conduction, adiabatic cooling behind the divergent shock, and the strong temperature dependence of the opacity.

The physics of matter under SL conditions is not yet understood with high precision. Our results, based on approximate thermodynamic and transport property models, suggest that the basic strategy of hydrodynamic code simulation is valid and that semiquantitative predictions are possible. Although it remains to be confirmed

experimentally that shock waves or plasmas are present in a bubble undergoing SL, no other model of which we are aware has been able to explain such a broad array of experimental data.

## REFERENCES AND NOTES

- D. F. Gaitan, thesis, University of Mississippi (1990).
- D. F. Gaitan *et al.*, *J. Acoust. Soc. Am.* **91**, 3166 (1992).
- B. P. Barber and S. J. Putterman, *Nature* **352**, 318 (1991).
- R. Hiller, S. J. Putterman, B. P. Barber, *Phys. Rev. Lett.* **69**, 1182 (1992).
- C. C. Wu and P. H. Roberts, *ibid.* **70**, 3424 (1993).
- W. C. Moss, D. B. Clarke, J. W. White, D. A. Young, *Phys. Fluids A* **6**, 2979 (1994).
- T. J. Matula *et al.*, in preparation.
- R. Hiller, K. Weninger, S. J. Putterman, B. P. Barber, *Science* **266**, 248 (1994).
- Ya. B. Zel'dovich and Yu. P. Raizer, *Physics of Shock Waves and High-Temperature Hydrodynamic Phenomena* (Academic Press, New York, 1966), chaps. I–III.
- D. Lohse *et al.*, *Phys. Rev. Lett.* **78**, 1359 (1997).
- T. J. Matula, unpublished data. No afterglow could be observed, even after gating out the main flash, to within the limits of the resolution of the equipment.
- Ya. B. Zel'dovich and Yu. P. Raizer, *Physics of Shock Waves and High-Temperature Hydrodynamic Phenomena* (Academic Press, New York, 1966), chaps. VI–VII.
- $T_i \neq T_e$  would be very important if we considered the possibilities for microthermonuclear fusion in a sonoluminescing  $\text{D}_2$  bubble, which requires ion temperatures exceeding 200 eV [W. C. Moss, D. B. Clarke, J. W. White, D. A. Young, *Phys. Lett. A* **211**, 69 (1996)].
- C. A. Iglesias and F. J. Rogers, personal communication.
- G. C. Pomraning, *The Equations of Radiation Hydrodynamics* (Pergamon, New York, 1973), pp. 44–49.
- R. Löfstedt *et al.*, *Phys. Fluids A* **5**, 2911 (1994) (figure 1).
- G. B. Zimmerman, *Lawrence Livermore Natl. Lab. Rep. UCRL-74811* (1973).
- J. von Neumann and R. D. Richtmyer, *J. Appl. Phys.* **21**, 232 (1950).
- J. W. White, *J. Comp. Phys.* **12**, 553 (1973).
- D. A. Young, unpublished results.
- \_\_\_\_\_ and E. M. Corey, *J. Appl. Phys.* **78**, 3748 (1995).
- W. C. Moss, *J. Acoust. Soc. Am.* **101**, 1187 (1997).
- F. J. Rogers, *Phys. Rev. A* **24**, 1531 (1981).
- Ya. B. Zel'dovich and Yu. P. Raizer, *Physics of Shock Waves and High-Temperature Hydrodynamic Phenomena* (Academic Press, New York, 1966), chap. V.
- W. H. Lokke and W. Grasberger, *Lawrence Livermore Natl. Lab. Rep. UCRL-52276* (1977).
- See (8), figure 4; B. P. Barber *et al.*, *Phys. Rev. Lett.* **74**, 5276 (1995) (figure 2); B. P. Barber *et al.*, *ibid.* **72**, 1380 (1994) (figure 2).
- We thank the B-Div. and the LASNEX code groups for technical and computational support. Computational support from J. Levatin, and technical critiques by J. White, T. Ladd, T. Gay, and especially T. Matula, are appreciated greatly. Funding was provided by N. Burkhard through the Lawrence Livermore National Laboratory (LLNL) Containment Program. This work was performed under the auspices of the U.S. Department of Energy by LLNL under contract W-7405-Eng-48.

7 February 1997; accepted 1 April 1997

## Block Copolymer Lithography: Periodic Arrays of $\sim 10^{11}$ Holes in 1 Square Centimeter

Miri Park, Christopher Harrison, Paul M. Chaikin,  
Richard A. Register, Douglas H. Adamson

Dense periodic arrays of holes and dots have been fabricated in a silicon nitride-coated silicon wafer. The holes are 20 nanometers across, 40 nanometers apart, and hexagonally ordered with a polygrain structure that has an average grain size of 10 by 10. Spin-coated diblock copolymer thin films with well-ordered spherical or cylindrical microdomains were used as the templates. The microdomain patterns were transferred directly to the underlying silicon nitride layer by two complementary techniques that resulted in opposite tones of the patterns. This process opens a route for nanometer-scale surface patterning by means of spontaneous self-assembly in synthetic materials on length scales that are difficult to obtain by standard semiconductor lithography techniques.

In general, feature sizes greater than 300 nm are routinely produced by photolithography techniques. For feature sizes between 300 and 30 nm, electron beam lithography is commonly used. However, feature sizes less than 30 nm are not easily obtained by

standard semiconductor lithography techniques. Because of the drive toward smaller, faster, and denser microelectronic systems, different novel techniques for nanolithography have been investigated by many researchers (1). Self-assembly in synthetic materials as a means of nanopatterning has also been proposed recently (2). Electronic circuits often require complex multilevel lithography, but in many devices, simple periodic patterning is sufficient. Various applications of nanometer periodic patterning would include the creation of a periodic

M. Park, C. Harrison, P. M. Chaikin, Department of Physics, Princeton University, Jadwin Hall, Princeton, NJ 08544, USA.

R. A. Register, Department of Chemical Engineering, Princeton University, Princeton, NJ 08544, USA.

D. H. Adamson, Princeton Materials Institute, Princeton University, Princeton, NJ 08544, USA.